Radiative Climate Forcing by the Mount Pinatubo Eruption

P. Minnis, E. F. Harrison, L. L. Stowe, G. G. Gibson, F. M. Denn, D. R. Doelling, W. L. Smith, Jr.

Radiative flux anomalies derived from the National Aeronautics and Space Administration (NASA) spaceborne Earth Radiation Budget Experiment were used to determine the volcanic radiative forcing that followed the eruption of Mount Pinatubo in June 1991. They are the first unambiguous, direct measurements of large-scale volcanic forcing. The volcanic aerosols caused a strong cooling effect immediately; the amount of cooling increased through September 1991 as shortwave forcing increased relative to the longwave forcing. The primary effects of the aerosols were a direct increase in albedo over mostly clear areas and both direct and indirect increases in the albedo of cloudy areas.

Volcanic activity has long been suspected to cause significant short-term climate changes. Powerful volcanic eruptions typically inject huge quantities of gases and ash into the stratosphere where they produce optically significant aerosols that may remain for several years. Because of their small size, these aerosols are more effective at reflecting shortwave solar radiation than they are at attenuating the longer wavelength, Earth-emitted radiation. Thus, the aerosols alter the Earth's radiation balance by reflecting more of the sun's energy back to space and permitting the Earth to cool radiatively at about the same rate as before the eruption. The result is a net loss of energy for the Earth atmosphere system, or a cooling of the atmosphere and surface. Clouds generally produce a similar effect but for somewhat different reasons (*1*).

The change in the Earth's radiation budget that is initiated by the eruptions is termed volcanic aerosol forcing or, more simply, volcanic forcing. Dust depletes some of the energy available to Earth's climate system, thereby forcing the system to adapt to reach a new equilibrium state. The response parameter usually measured is air or sea surface temperature. Numerous attempts that have been made to relate global temperature trends to volcanism have produced mixed results (*2*). Efforts to quantify the volcanic forcing have been hampered by a lack of data. Reductions in solar radiation at the surface that were measured at only a few locations have been used to infer qualitatively the alteration of the global radiation budget (*3*). An attempt to quantify the radiative perturbations by the 1982 El Chichón eruption with the use of Nimbus-7 satellite data was inconclusive (*4*). The most common method of estimating volcanic forcing is to calculate the radiative transfer on the basis of assumptions or measurements of aerosols and their optical properties (*5*). These properties, spatial distributions, and lifetimes of volcanically derived stratospheric aerosols are quite variable, so theoretical results suffer from large uncertainties.

Beginning 12 June 1991, a series of spectacular eruptions of the Mount Pinatubo volcano (15.1°N, 120.3°E) in the Philippines produced the greatest ash clouds that have been observed since the beginning of the satellite era. This event, while catastrophic for the people living in the vicinity of Mount Pinatubo, presents the opportunity for an experiment in climate change. In this article, we analyze direct satellite measurements of the radiation budget as well as the optical properties of the aerosols to quantify the volcanic forcing of the Earth's climate.

P. Minnis and E. F. Harrison are with the Atmospheric Sciences Division, National Aeronautics and Space Administration, Langley Research Center, Hampton, VA 23681. L. L. Stowe is with the National Environmental Satellite, Data, and Information Service, National Oceanic and Atmospheric Administration, Camp Springs, MD 20233. G. G. Gibson, F. M. Denn, D. R. Doelling, and W. L. Smith, Jr., are with Lockheed Engineering and Sciences Company, Hampton, VA 23666.

Observations

Data from the NASA Earth Radiation Budget Satellite (ERBS) Stratospheric Aerosol and Gas Experiment (SAGE II) have shown that the stratospheric aerosol optical depth increased by up to two orders of magnitude between 40°N and 40°S during the first 5 months after the initial eruptions of Mount Pinatubo (*6*). Analyses of National Oceanic and Atmospheric Administration (NOAA)–11 Advanced Very High Resolution Radiometer (AVHRR) data showed that the volcanic cloud spread inhomogeneously, increasing the total atmospheric aerosol optical depth over the tropical Pacific by a factor of 5 to an average value of ~0.35 by mid-August (*7*). For the assumption of continued spreading, it was estimated (*7*) that the volcanic debris would reduce the global clear-sky net radiation balance by 2.5 W m^{-2}. In addition, when cloudy areas were taken into account, the debris was expected to produce a cooling effect equivalent to about 0.5°C over the next 2 to 4 years. Data from the Nimbus-7 Total Ozone Mapping Spectrometer were used to infer that the mass of SO_2, the primary volcanic aerosol source in the stratosphere, that was injected by Mount Pinatubo was almost three times that of the 1982 El Chichón eruption in Mexico, which was the next largest volcanic cloud observed by satellites (*8*). Computer simulations have also been performed to estimate the global climatic impact of the Pinatubo eruptions (*9*). Assuming an aerosol loading 1.7 times that of El Chichón, researchers calculated that the global mean volcanic forcing would rise rapidly to a maximum value of ~4.5 W m^{-2} by early 1992 and decay exponentially to negligible values by 1995. The corresponding decreases in the simulated mean global surface air temperatures were predicted to reach a maximum value of 0.5°C in late 1992 before returning to normal by mid-1995.

These measurements and calculations provide critical information about the nature of the Pinatubo aerosols and their potential effects on the Earth's radiation budget and, ultimately, the surface climate. However, the calculations and early data contain many uncertainties (*9*). Much of the uncertainty in the volcanic forcing can now be minimized because the forcing can be directly measured from space with the use of the Earth Radiation Budget Experiment (ERBE) instruments on the ERBS.

The ERBE (*10*), equipped with a wide field of view (WFOV, ~1000-km resolution) radiometer, measures reflected shortwave (SW, 0.2 to 5.0 μm) and total outgoing (0.2 to 50.0 μm) radiation. The monthly means of outgoing longwave (LW = total − SW) and reflected SW fluxes are M_{LW} and M_{SW}, respectively. The monthly mean albedo and net radiation are

$$\alpha = M_{SW}/M_{SUN} \quad (1)$$

and

$$M_{NET} = (M_{SUN} - M_{SW}) - M_{LW} \quad (2)$$

respectively, where M_{SUN} is the mean incoming solar radiation for the month. Thus, if M_{SW} increases, M_{NET} decreases

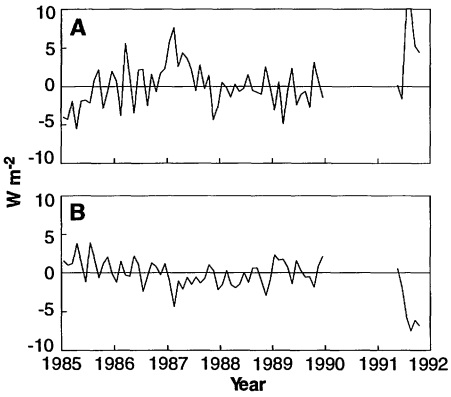

Fig. 1. Time series of ERBE (**A**) shortwave and (**B**) net flux anomalies relative to 5-year (1985 to 1989) monthly means for 5°N to 5°S.

and the area undergoes radiative cooling. Conversely, if M_{LW} decreases, the area warms radiatively.

To determine if relative cooling or warming occurs for a given month, it is necessary to know the long-term mean conditions for the same area and month. We represented these conditions by the average ERBS monthly means for 1985 through 1989. All analyses were limited to the areas between 40°N and 40°S because of the sampling characteristics of the ERBS. The difference between a given monthly mean and its corresponding 5-year monthly average is an anomaly. The SD in a quantity over the 5-year base-line period is a measure of the natural interannual variability without volcanic forcing. The accuracy of volcanic forcing for each month is given by the SD in the 5-year mean.

Variations in Large-Scale Flux

Because Pinatubo aerosols spread around the entire globe, we examined zonal variations relative to the 5-year mean to determine the strength of the perturbations. The increase in M_{SW} (Fig. 1A) associated with the Mount Pinatubo aerosols in August 1991 was 10 W m^{-2} between 5°N and 5°S. In the LW, the signal was barely detectable above the noise of interannual variability. In the time series of M_{NET} (Fig. 1B), a net cooling of almost 8 W m^{-2} occurred by

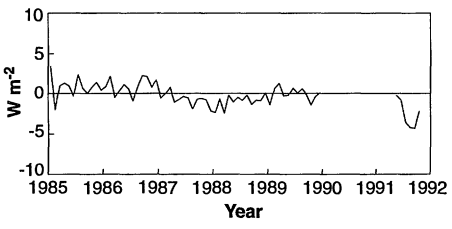

Fig. 2. Time series of ERBE net flux anomalies relative to 5-year (1985 to 1989) monthly means for 40°N to 40°S.

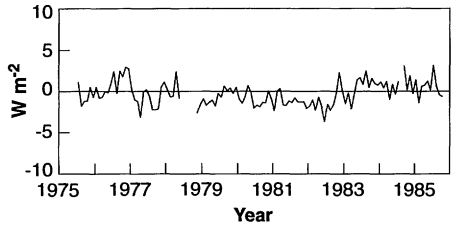

Fig. 3. Time series of Nimbus-6 and -7 net flux anomalies relative to 11-year (1975 to 1986) monthly means for 40°N to 40°S.

August 1991, twice the value of any other monthly anomaly. This trend continued for the zone between 40°N and 40°S (Fig. 2) with a net forcing of −4.3 W m^{-2} (cooling) for August 1991. The closest comparable anomaly was a net heating of 2.5 W m^{-2} during late 1986. Because the SD about the mean net flux for the zone is 1.5 W m^{-2}, the difference from the 5-year mean net flux that was observed during August 1991 is statistically significant at a 99% confidence level.

Globally, if the radiation budget for the Earth poleward of the 40° latitudes was unaffected by the volcanic clouds and if the anomalies resulted from the eruption, then the radiative cooling caused by Mount Pinatubo during August and September 1991 was 2.7 ± 1.0 W m^{-2}. However, this value represents the minimum effect because the enhanced stratospheric aerosols were observed at higher latitudes by mid-August (*6, 7, 11*).

Comparison of short-term data with long-term data also shows that volcanic aerosols produced a dramatic effect. Earth radiation budget WFOV sensors have been operating on the Nimbus-6 satellite, which is in a near-noon, sun-synchronous orbit, since 1975 and on the Nimbus-7 since 1978 (*12*). Data from the two satellites (*13*) were made compatible by removal of the trends from the Nimbus-6 SW values and normalization of the results to the mean from the Nimbus-7 data for 1978 to 1986. The results were used to compute anomalies in

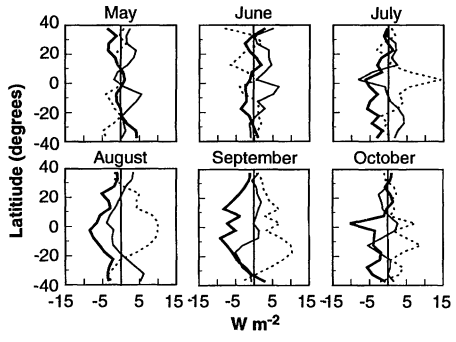

Fig. 4. Zonal radiative anomalies from ERBE for May to October 1991 (LW, solid line; SW, dashed line; and NET, heavy solid line).

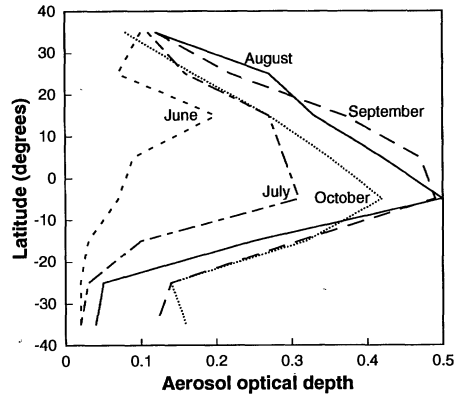

Fig. 5. Zonal mean aerosol optical depths from AVHRR for 5 months after the eruption of Mount Pinatubo (June to October 1991).

M_{NET} for the period between 1975 and 1986 covering the zone between 40°N and 40°S (Fig. 3). The SD in the anomalies is 1.5 W m^{-2}, the same value that we found for the 5-year ERBE data set. Thus, we conclude that the reference statistics for ERBE are typical for intervals of at least 11 years. The largest net flux anomaly found before the Pinatubo period occurred during June 1982 (3.5 W m^{-2}) which followed the April 1982 El Chichón eruption. That anomaly, which was only 2.6 W m^{-2} lower than the value for the previous months, persisted for only 1 month. The period during 1976 and 1977 had anomalies of ±3 W m^{-2}. Some of the variability in the Nimbus-6 data may have resulted from diminished sampling compared to that for Nimbus-7 (*13*). Even with the uncertainties in the Nimbus Earth radiation budget data, the net radiation anomalies after the Mount Pinatubo eruption were clearly the largest that have been observed from satellites.

Zonal Distribution of Forcing

The distribution and amount of observed forcing closely followed the spread of the aerosol cloud and the assumed progress of the chemical reactions within it. During May and June, the zonal anomalies for all three fluxes were generally within the interannual variability of ±3 W m^{-2} for the area between 40°N and 40°S (Fig. 4). The SW

Table 1. Linear regression slopes, *m*, for monthly mean zonal flux anomalies and aerosol optical depths, τ.

Month	τ	*m*(SW)	*m*(LW)	*m*(NET)
July	0.17	20.5	−17.6	−2.3
August	0.26	21.3	−16.8	−10.0
September	0.29	11.5	5.3	−16.4
October	0.25	13.2	−3.1	−15.1
Average	0.24	17.1	−7.9	−11.5

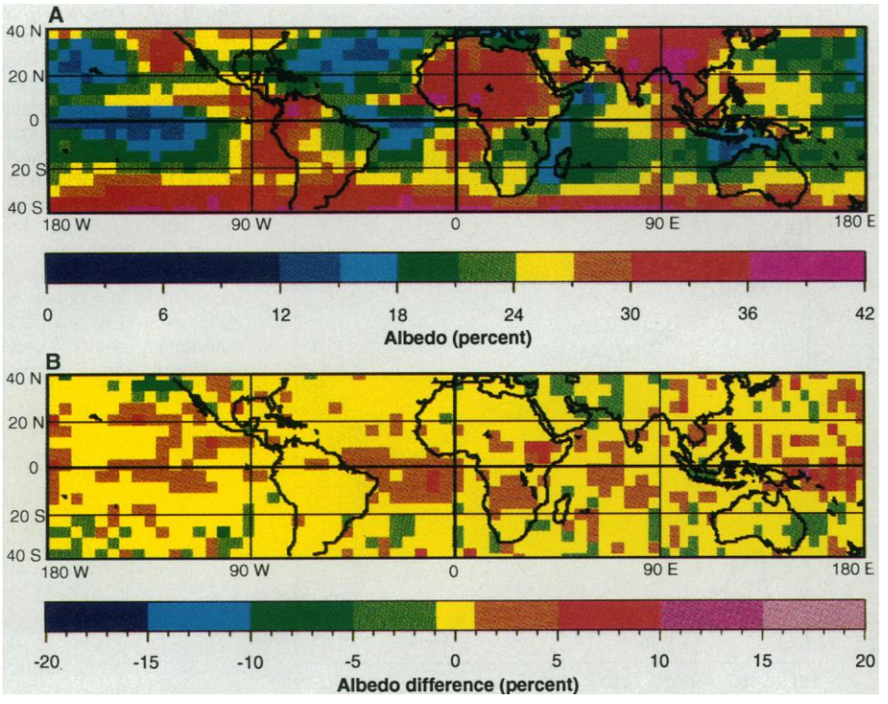

Fig. 6. (**A**) Average August albedo from ERBE for 5 years (1985 to 1989) and (**B**) difference in August 1991 albedo from the 5-year average. Regional differences smaller than their 5-year standard deviation were set to zero to enhance display of the more significant variations. Vegetated land and ocean areas that are generally cloud-free are those in (A) with $\alpha < 0.21$ (blue and dark green).

component increased dramatically over the equatorial belt during July, whereas that of the LW showed a corresponding decrease. By August, the latitudinal spreading of the volcanic cloud was apparent in the positive SW anomalies from 30°N to 20°S. An opposite effect of smaller magnitude was evident in the LW data, resulting in significant negative anomalies in M_{NET}. The strongest effects continued between 10°N and 30°S during September and October. These anomalies are consistent with the changes in the magnitude and horizontal distribution of the volcanic cloud. The volcanic debris, which contained massive amounts of SO_2 (*8*), probably generated large quantities of sulfate aerosols during the first 2 months after the eruption (*14*, *15*).

During June, the aerosol enhancement was mainly confined to a 15° zone centered at 15°N, the latitude of Mount Pinatubo (Fig. 5). Spatial analyses indicate that the June enhancement includes the effects of both Saharan dust and the Pinatubo aerosols. As the Mount Pinatubo aerosols spread during subsequent months, the zone of maximum optical depth moved slightly south of the equator. The peak optical depths in August and September were nearly identical, whereas optical depths in October indicate that the effluent loading was declining.

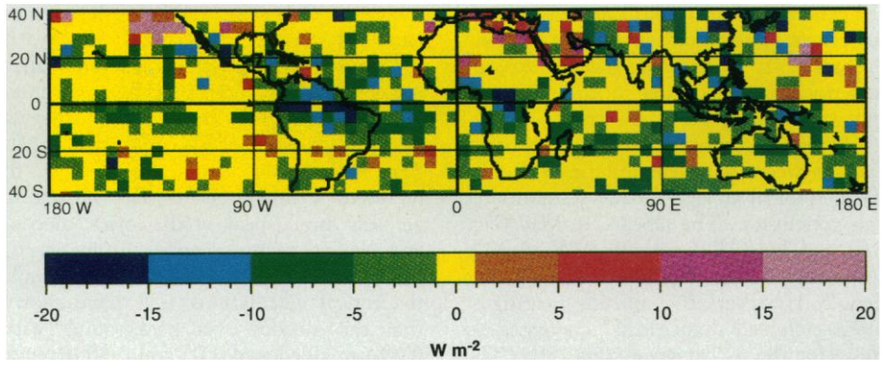

Fig. 7. Difference in ERBE net radiation between 1991 and the 5-year average for August. Regional differences smaller than their 5-year standard deviation were set to zero to enhance display of the more significant variations.

The changes in the distribution of aerosols were temporally and spatially associated with variations in radiative flux (Fig. 4). For the purposes of comparison and to produce the best correlations, we assumed that the relation between zonal mean optical depths, τ, and radiative flux anomalies is linear. For this model, the regression fit

$$\Delta SW = (17.1 \pm 5.6)\tau - 0.7 \quad (3)$$

for the SW data and

$$\Delta LW = (-7.9 \pm 5.1)\tau + 1.9 \quad (4)$$

for the LW data. The fit to the net radiative forcing data

$$\Delta NET = (-11.5 \pm 4.4)\tau - 0.5 \quad (5)$$

The uncertainties in the slopes, given for the 90% confidence level, arise from many factors, especially the interannual variability that is superimposed on the volcanic forcing.

The ERBE data reflect the climate sensitivity that was averaged over the first 4 months after the eruption. After any eruption, the largest ash particles settle out during the first few months and the sulfuric gases form small sulfate aerosols. For example, the size distributions of stratospheric aerosols that were measured after the El Chichón eruption (*16*) showed that particle size decreased from an effective radius of ~1.4 μm that was observed 1.5 months after the eruption to ~0.5 μm after 6.5 months. Such a change in aerosol size should have a considerable effect on the volcanic forcing. According to theoretical calculations (*17*), SW forcing dominates and the net volcanic forcing is negative when the effective radius of the stratospheric particles is less than 2.2 μm. For larger particle sizes, the LW forcing dominates and the system undergoes warming. Thus, the LW effect should be greatest relative to that of the SW soon after the eruption. This change in sensitivity with time can be estimated with the slopes, m, from a simple linear fit to the data (Table 1). During July, m(SW) was 20% greater than m(LW). The ratio $|m(\text{SW})/m(\text{LW})|$ increased through October, although m(NET) leveled out during September. The increase in $|m(\text{NET})|$ is consistent with decreasing particle size from July to October.

If we assume that the 4-month mean of the aerosol size distribution from Mount Pinatubo is similar to that observed 1.5 months after the El Chichón eruption, the theoretical model (*17*) predicts a net forcing of -2.8 W m^{-2} for a global mean of the aerosol optical depth of 0.15 (*18*). The

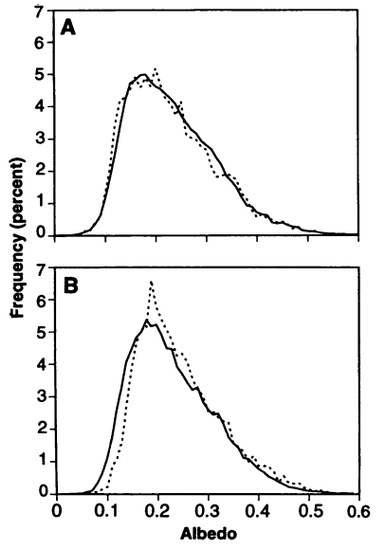

Fig. 8. Five-year (1985 to 1989, solid line) and 1991 (dotted line) daily mean albedo histograms from ERBE for (**A**) May and (**B**) August (30°N to 30°S).

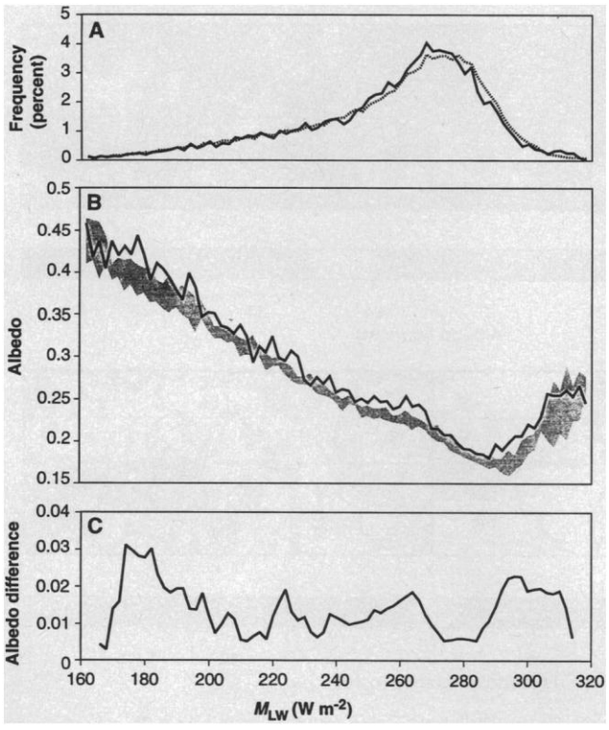

Fig. 9. (**A**) Frequency of occurrence of daily mean LW flux (1991, solid line; 1985 to 1989, dotted line), (**B**) average daily mean albedo as a function of daily mean LW flux [1991, solid line; 1985 to 1989, shaded region (mean ± SD)], and (**C**) difference between the 1991 and the 5-year average daily mean albedos as a function of daily mean LW flux. The differences have been smoothed with a 5-point running mean.

empirical model (Eq. 5) yields -2.3 ± 0.6 W m^{-2} for the same optical depth, whereas the anomaly derived directly from the data is -2.7 ± 1.0 W m^{-2}. Thus, the theoretical calculations produce a net forcing within the uncertainty limits of results derived from ERBE for the initial Mount Pinatubo post-eruption period.

Regional Distribution of Forcing

Even within a given latitude zone, the volcanic effects were not evenly distributed. For example, the 5-year mean August albedos (Fig. 6A) were generally smaller than the August 1991 albedos between 30°N and 30°S (Fig. 6B), especially over the clearest areas. The greatest differences were found over the central Pacific and Atlantic oceans, over the Congo basin, and in the vicinity of New Guinea. Differences for the 30° to 40° latitude zones were more variable.

Net radiation south of 30°N was significantly less during August 1991 (Fig. 7) than in August from 1985 to 1989. The greatest and most extensive cooling effect occurred over the Amazon and Congo basins and over the central equatorial Atlantic and Pacific oceans. These ocean areas tend to have the fewest clouds, whereas the Amazon and Congo frequently have deep convective storms (*19*). Other regions with low mean cloud amounts, including central Australia, New Guinea, Madagascar, and the sea east of Africa, also showed a significant decrease in net radiation. Except for the Mediterranean Sea and the Arabian Peninsula, large areas where significant changes in radiation occurred poleward of 30° usually have relatively high albedos (Fig. 6A) and are typically quite cloudy. The increased net radiation over the Arabian Peninsula, apparently a result of the Kuwaiti oil fires (*20*), persisted but diminished in intensity from May through October 1991.

Pinatubo's effect was most evident over areas that tend to be cloud-free. A small rise in atmospheric optical depth substantially increases the system albedo over a relatively dark surface but has a smaller impact on the total albedo over brighter surfaces (*14*) such as clouds, light sand, or alkali deserts. Thus, the apparent lack of a significant signal over the Sahara is not surprising, and the increased albedo over the much darker deserts of Australia is expected for an optically thicker atmosphere. Because it is improbable that all of the generally clear, tropical regions suddenly became more cloudy than normal during August 1991, we conclude that the volcanic aerosols are responsible for the enhanced radiative cooling over these areas.

A comparison of the frequency distributions between the 5-year and the 1991 daily mean tropical albedos further substantiates this conclusion. The albedos in May (Fig. 8A) and June 1991 for the 30°N to 30°S zone were similar to those for the 5-year period. However, the albedos in August 1991 increased dramatically compared to those for the 5-year mean (Fig. 8B). The minimum albedos, corresponding to cloud-free regions, increased by 0.02 for August 1991. There was also a statistically significant increase (1 to 2 SDs about the 5-year means) in the number of large albedos ($0.36 < \alpha < 0.52$) that correspond to thick convective cloud systems and to some low-level stratus decks. Overall, August albedos were 0.014 (5.6 SDs) greater than the 5-year mean of 0.236. The albedo increases for July and September were similar to those for August, but those for October were somewhat smaller. Although the mean LW fluxes for May through October 1991 were within 1 SD of the monthly mean of the tropical 5-year LW fluxes, the mean daily LW fluxes for August that are associated with low clouds or generally cloud-free areas were slightly less than the corresponding 5-year norm (Fig. 9A). There were no differences among the frequencies of the LW fluxes for cloudy or mostly cloudy regions, which suggests that there was no increased convective activity during the period of interest.

Aerosols can alter the radiation balance either directly by increasing the atmospheric optical depth or indirectly by altering cloud microphysical characteristics (*21*). The enhanced clear-sky albedos (Fig. 6) represent a direct effect. The impact of aerosols should peak at the lowest albedos and decrease monotonically with increasing background albedo. For example, simple theoretical calculations (*14*) have shown that the albedos over backgrounds with 0.50-μm albedos of 0.05 and 0.30 increase by 0.052 and 0.032, respectively, when a volcanic aerosol layer is inserted above the background. The trend would be the same

for the broad-band SW albedos. However, the magnitude of the changes would be smaller because of absorption at selected wavelengths and diminished scattering efficiencies at longer wavelengths.

The variations of daily mean albedo with LW flux during August 1991 compared with those for the 5-year period between 1985 and 1989 (Fig. 9, B and C) show some evidence of the trend that is expected from the direct effect. The albedo increase for both the clearest ocean ($M_{LW} \approx 295$ W m^{-2}) and land areas ($M_{LW} \approx 305$ W m^{-2}) was 0.022 (Fig. 9C). After a sharp drop to 0.006 at $M_{LW} \approx 280$ W m^{-2} and a recovery to 0.020 at $M_{LW} \approx 260$ W m^{-2}, the differences exhibit a generally downward trend to reflect relatively cloudy scenes ($M_{LW} \approx 220$ W m^{-2} and $\alpha \approx 0.290$). The albedo differences tend to increase, however, with decreasing LW fluxes for $M_{LW} < 220$ W m^{-2}. The greatest albedo differences occurred for deep convective clouds ($M_{LW} \approx 175$ W m^{-2}). The reversed trend in albedo differences at the lower LW fluxes is inconsistent with the direct effect. This reversal suggests that the aerosol layer caused an indirect effect on the albedo by altering the microphysical characteristics of the deeper convective clouds. Such changes may explain why the largest decreases in net radiation occurred over the tropical convective storm regions (Fig. 7).

After an eruption, volcanic debris in the stratosphere filters into the lower stratosphere and troposphere, primarily in the vicinity of tall convective storms and in tropopause folds. Significantly enhanced tropospheric aerosol loading due to Mount Pinatubo was observed by lidars as far north as 40°N during August 1991 (*22*). Thus, significant amounts of volcanic aerosols were available for incorporation into the clouds, especially at the upper levels. Sulfate aerosols function as efficient cloud condensation nuclei, and volcanic ash can act as an ice nucleus at temperatures below −16°C (*23*). Greater concentrations of cloud and ice nuclei tend to increase the number and reduce the effective radius of the hydrometeors in the cloud (*21*). If a cloud has a constant liquid or ice water content, its albedo increases as the effective particle radius decreases (*21, 24*). This indirect effect could explain the increased albedos for the LW fluxes that correspond to deep convective clouds without changing the LW flux, because optically thick (high-albedo) clouds are opaque to LW radiation. Although the indirect effects are most noticeable for deep clouds (that is, $M_{LW} < 220$ W m^{-2}), they may also occur for other cloud types. For example, diffusion of volcanic aerosols across the tropopause may alter the optical properties of high, thin cirrus clouds or enhance the generation of clouds (*25*).

Volcanic radiative impacts are more complex than the model that depicts direct forcing by a single aerosol layer that is distributed uniformly over the background. Indirect effects are not now included in most climate models. These results provide additional impetus to include indirect aerosol effects such as variable cloud particle size in climate prediction models.

REFERENCES AND NOTES

1. V. Ramanathan *et al.*, *Science* **243**, 57 (1989).
2. H. W. Ellsaesser, *Mon. Weather Rev.* **105**, 1200 (1977); P. M. Kelly and C. B. Sear, *Nature* **311**, 740 (1984); H. H. Lamb, *Philos. Trans. R. Soc. London* **266**, 425 (1970); H. E. Landsberg and J. M. Albert, *Weatherwise* **27**, 63 (1974); J. K. Angell and J. Korshover, *Mon. Weather Rev.* **112**, 1457 (1984); C. F. Mass and D. A. Portman, *J. Clim.* **2**, 566 (1989).
3. A. J. Dyer and B. B. Hicks, *Nature* **208**, 131 (1965); H. J. Viebrock and E. C. Flowers, *Tellus* **20**, 400 (1968); G. Wendler, *Bull. Am. Meteorol. Soc.* **65**, 216 (1984).
4. P. E. Ardanuy and H. L. Kyle, *J. Clim. Appl. Meteorol.* **25**, 505 (1986).
5. J. B. Pollack *et al.*, *J. Geophys. Res.* **81**, 1071 (1976); Harshvardhan, *J. Atmos. Sci.* **36**, 1274 (1979); L. D. D. Harvey and S. H. Schneider, *J. Geophys. Res.* **90**, 2207 (1985).
6. M. P. McCormick and R. E. Veiga, *Geophys. Res. Lett.* **19**, 155 (1992). The ERBS was launched in 1984 into a 57° inclination orbit with an altitude of 600 km. It carries the ERBE instruments for measurement of top-of-atmosphere radiative flux and the SAGE II, which measures vertical profiles of aerosol extinction in the atmosphere by viewing the sun during sunrise or sunset relative to the satellite. Stratospheric optical depth is obtained by integration of the extinction profile from the tropopause to 40 km.
7. L. L. Stowe *et al.*, *Geophys. Res. Lett.* **19**, 159 (1992).
8. G. J. S. Bluth *et al.*, *ibid.*, p. 151.
9. J. Hansen *et al.*, *ibid.*, p. 215.
10. B. R. Barkstrom, *Bull. Am. Meteorol. Soc.* **65**, 1170 (1984).
11. H. Jager, *Geophys. Res. Lett.* **19**, 191 (1992); P. V. Johnston *et al.*, *ibid.*, p. 211; P. J. Sheridan *et al.*, *ibid.*, p. 203.
12. W. L. Smith *et al.*, *Appl. Opt.* **16**, 306 (1977); H. Jacobowitz *et al.*, *J. Geophys. Res.* **89**, 5021 (1984).
13. T. D. Bess and G. L. Smith, *NASA Ref. Publ. 1185* (1987); *NASA Ref. Publ. 1186* (1987); G. L. Smith *et al.*, *NASA Ref. Publ. 1230* (1990); G. L. Smith *et al.*, *NASA Ref. Publ. 1231* (1990).
14. F. P. J. Valero and P. Pilewskie, *Geophys. Res. Lett.* **19**, 163 (1992).
15. T. Deshler *et al.*, *ibid.*, p. 199; A. Goldman *et al.*, *ibid.*, p. 183; R. M. Hoff, *ibid.*, p. 175.
16. D. J. Hofman and J. M. Rosen, *Science* **222**, 325 (1983).
17. A. Lacis *et al.*, *Geophys. Res. Lett.* **19**, 1607 (1992).
18. We estimated this value of optical depth by spreading the 4-month mean optical depth in Table 1 around the globe, assuming that the aerosol effects were confined between 40°N and 40°S.
19. S. G. Warren *et al.*, *National Center for Atmospheric Research Technical Note 273+STR* (1986); S. G. Warren *et al.*, *National Center for Atmospheric Research Technical Note 317+STR* (1988).
20. S. S. Limaye *et al.*, *J. Geophys. Res.* **97**, 14551 (1992).
21. R. J. Charlson *et al.*, *Science* **255**, 423 (1992).
22. M. J. Post *et al.*, *Geophys. Res. Lett.* **19**, 195 (1992).
23. B. J. Mason and J. Maybank, *Q. J. R. Meteorol. Soc.* **84**, 235 (1958); V. J. Schaeffer, *Chem. Rev.* **44**, 291 (1949).
24. P. Minnis, thesis, University of Utah (1991).
25. K. Sassen, *Science* **257**, 516 (1992).

26. We thank J. F. Kibler and the ERBE Data Management Team for their efforts in processing the ERBE data as well as R. D. Cess, D. F. Young, and the anonymous reviewers for their valuable comments and suggestions.

Molecular Matchmakers

Aziz Sancar and John E. Hearst

Molecular matchmakers are a class of proteins that use the energy released from the hydrolysis of adenosine triphosphate to cause a conformational change in one or both components of a DNA binding protein pair to promote formation of a metastable DNA-protein complex. After matchmaking the matchmaker dissociates from the complex, permitting the matched protein to engage in other protein-protein interactions to bring about the effector function. Matchmaking is most commonly used under circumstances that require targeted, high-avidity DNA binding without relying solely on sequence specificity. Molecular matchmaking is an extensively used mechanism in repair, replication, and transcription and most likely in recombination and transposition reactions, too.

In the 1960s and 1970s models were proposed for protein folding and for binding of proteins to DNA. According to these models, proteins folded by following a kinetic pathway dictated by their primary structures (*1*); similarly, it was proposed that DNA binding proteins bound to specific sequences on DNA by presenting a set of hydrogen bond donors and acceptors complementary to those in the major or minor groove of the recognition sequences (*2*). The research of the past 25 years has generally supported these models (*3*). However, in recent years evidence has accumulat-

A. Sancar is in the Department of Biochemistry and Biophysics, University of North Carolina School of Medicine, Chapel Hill, NC 27599. J. E. Hearst is in the Department of Chemistry and the Division of Chemical Biodynamics, Lawrence Berkeley Laboratory, University of California, Berkeley, CA 94720.